Nonlinear internal wave at the interface of two-layer liquid due to a moving hydrofoil

wang, zhen; Wu, CH; Zhou, Li; Wang, Qian

DOI:
10.1063/1.4993460

Nonlinear internal wave at the interface of two-layer liquid due to a moving hydrofoil

Zhen Wang, Changhong Wu, Li Zou, Qianxi Wang, and Qi Ding

Citation: Physics of Fluids **29**, 072107 (2017);
View online: https://doi.org/10.1063/1.4993460
View Table of Contents: http://aip.scitation.org/toc/phf/29/7
Published by the American Institute of Physics

Nonlinear internal wave at the interface of two-layer liquid due to a moving hydrofoil

Zhen Wang,[1,a)] Changhong Wu,[1] Li Zou,[2,a)] Qianxi Wang,[2,3] and Qi Ding[1]
[1]*School of Mathematical Sciences, Dalian University of Technology, Dalian 116024, China*
[2]*School of Naval Architecture, Dalian University of Technology, Dalian 116024, China*
[3]*School of Mathematics, University of Birmingham, Birmingham B15 2TT, United Kingdom*

(Received 25 February 2017; accepted 24 June 2017; published online 18 July 2017)

This paper is concerned with the internal wave at the interface of two layers of liquids due to a hydrofoil in the lower layer liquid. The two-layer fluid is assumed moving parallel to the interface at different velocities. The stratified flow is modeled based on the incompressible potential flow theory, with the nonlinear boundary conditions at the interface. Boundary integral equations are formulated for the fully nonlinear interfacial wave generated by the hydrofoil. The numerical model results in a set of nonlinear algebra equations, which are solved using the quasi-Newton method. We show that the quasi-Newton method is more efficient than Newton's method, which is often used for solving these types of equations in the literature. The wave profiles were analyzed in terms of the location and thickness of the hydrofoil, the Froude number, and the ratio of the densities of the two fluids. The computations show that the interfacial wave amplitude showed a trend first of increase and then of decrease with the distance between the hydrofoil and the still interface. *Published by AIP Publishing.* [http://dx.doi.org/10.1063/1.4993460]

I. INTRODUCTION

A stratified flow with varying density, due to variations of temperature, salinity, and pressure, along with depth, is a common phenomenon in the oceans. When a stratified flow encounters disturbances, such as uneven topography, tides, and atmospheric disturbances, internal waves are generated.[1–4] Internal waves change the temperature and salinity field.[5–7] In addition, they have important dynamic effects on offshore structures such as oil platforms, pipes lying on the seabed, and submarines. Due to the wide applications of internal waves in engineering and the atmospheric and oceanographic sciences,[8,9] the generation and propagation of the internal waves attract many researchers to explore.[10,11]

The simple two-layer fluid model is often used to study a stratified flow. The interfacial waves between two layers can be described by the Korteweg-de Vries (KdV) type equations under the weak nonlinear assumption.[11] Alam *et al.*[12] studied the translation of an oscillatory disturbance in a two-layer density stratified fluid using the Green functions for two- and three-dimensional configurations.

A hydrofoil moving in a single-layer liquid has been well studied based on the potential flow theory, with the linear and nonlinear boundary conditions at the free surface.[13,14] Prasad[15] simulated unsteady planar viscous flows generated by a hydrofoil moving beneath a free surface. Lacaze[16] investigated gravity waves generated by a moving obstacle in a two-layer stratified fluid by experiments.

Under the assumption of ideal fluids, Forbes established a boundary integral equation to describe the fully nonlinear flow over a semicircular obstacle.[17] Forbes also studied wave resistance of a semi-elliptical body and the nonlinear drag-free flow.[18,19] Forbes modeled two-layer flows over a semi-circular obstruction and an arbitrary topography.[20,21] Melville and Helfrich[22] analyzed a transcritical two-layer flow over the given topograph. Dias and Vanden-Broeck investigated the trapped waves between two submerged obstacles.[23] Page and Parau studied the hydraulic falls under a floating ice plate due to submerged obstructions.[24] Parau *et al.*[25] simulated the time evolution of three-dimensional nonlinear gravity-capillary free surface flows. Wang[26] simulated three-dimensional nonlinear waves using the boundary integral method with an unstructured mesh.

A point source and vortex induced internal waves are studied using the boundary integral methods.[27–30] Forbes[31] modelled the free surface wave due to a moving hydrofoil using the potential flow theory coupled with complex analyses. It results in an integral-differential equation, which was simulated by using Newton's method. Forbes and Hocking used the quasi-Newton method in a reasonably large-scale calculation of a three-dimensional flow due to a sink near a vertical wall.[32] Pethiyagoda, McCue, and Moroney[33] used iterative methods to update the Jacobian matrix so as to reduce computer run-time.

In this paper, we develop the boundary integral method[31,34] for modelling internal waves at the interface of a two-layer liquid, due to a hydrofoil beneath the interface. We formulate three integral-differential equations for potential flows in the upper and lower layers. The physical and mathematical model is described based on the potential flow theory and complex analyses in Sec. II. In Sec. III, the numerical model is formulated based on the quasi-Newton method. Numerical simulations of the internal waves due to

a)Authors to whom correspondence should be addressed: wangzhen@dlut.edu.cn and lizou@dlut.edu.cn

a moving hydrofoil beneath the interface are presented in Sec. IV.

II. FORMULATION OF THE PROBLEM

Consider two layers of liquids with different densities, moving horizontally at the same direction with velocities, as sketched in Fig. 1. A Cartesian coordinate system is defined such that the x-axis is along the moving direction of the stream and at the level of undisturbed interface, and y-axis is located upwards vertically. It is assumed that the flows at both layers are incompressible and potential. The liquid at the upper layer has a density ρ_1 and velocity c_1 at far field, while the liquid at the lower layer has a density ρ_2 and velocity c_2. We only consider the stable case for which ρ_2 is bigger than ρ_1. The rigid lid assumption is utilized to the surface of the upper layer, which has finite depth T. The subscripts 1 and 2 are related to variables or parameters associated with the upper layer and lower layer, respectively.

The length and the thickness of the hydrofoil are denoted as $2L$ and $2B$, respectively, with its center of gravity located at the depth H beneath the undisturbed interface. The upper and lower surfaces of the hydrofoil are described as $y = b_{\pm}(x)$, $-L \le x \le L$. The disturbed interface is described by $y = \eta(x)$. The problem can be formulated in a dimensionless form with the reference velocity c_2 and reference hydrofoil half-length L. The velocity potentials $\phi_j, j = 1, 2$ and stream functions $\psi_j, j = 1, 2$ are normalized by $c_2 L$. We choose $\psi_1 = \psi_2 = 0$ on the interface and $\phi_1 = \phi_2 = 0$ at the point of $x = 0$ at $t = 0$ on the interface without loss of generality. With the nondimensionalization, we obtain the following dimensionless parameters:

$$F = \frac{c_2}{\sqrt{gL}}, \quad h = \frac{H}{L}, \quad \beta = \frac{B}{L},$$

$$\theta = \frac{T}{L}, \quad \rho = \frac{\rho_1}{\rho_2}, \quad \gamma = \frac{c_1}{c_2},$$

where F is the Froude number for the flow in the lower layer. In the rest of the paper, all variables are dimensionless.

To analyze the problem using the complex variable theory, we introduce complex potential $f_j = \phi_j + \mathrm{i}\psi_j, j = 1, 2$ in terms of $z = x + \mathrm{i}y$, where $\mathrm{i} = \sqrt{-1}$. According to the potential theory, the stream functions and velocity potentials satisfy the Cauchy-Riemann equations,

$$\frac{\partial \phi_j}{\partial x} = \frac{\partial \psi_j}{\partial y}, \quad \frac{\partial \phi_j}{\partial y} = -\frac{\partial \psi_j}{\partial x}, j = 1, 2. \tag{1}$$

The far field conditions read

$$f_1 \to \gamma z, f_2 \to z, \quad \text{as} \quad \mathrm{Re}(z) \to -\infty, \tag{2}$$

where Re() denotes the real part of its variable. No-penetration condition on the rigid lid $y = \theta$ is

$$\nabla \phi_1 \cdot \mathbf{n} = 0. \tag{3}$$

The kinematic boundary condition, at the interface $y = \eta(x)$, is that the normal velocity component is zero,

$$\nabla \phi_j \cdot \mathbf{n} = 0, \quad j = 1, 2. \tag{4}$$

The non-penetration boundary conditions on the surface of the hydrofoil is

$$v_{\pm} = u_{\pm} b'_{\pm}(x) \quad \text{for} \quad y = b_{\pm}(x), \quad -1 \leqslant x \leqslant 1, \tag{5}$$

where the subscripts "+" and "–" denote the upper and lower surfaces of the hydrofoil, respectively.

For illustration purpose, we will consider a hydrofoil defined by the following equation:

$$b_{\pm}(x) = -h \pm \frac{3}{4}\beta(1 - x)\sqrt{\frac{3}{2}(1 + x)}, \quad \text{as} \quad -1 \leqslant x \leqslant 1. \tag{6}$$

The hydrofoil has a blunt nose and a cusped trailing edge, achieving its maximum width 2β for $x = -\frac{1}{3}$. At the trailing edge, the Kutta condition is imposed as follows:[31]

$$u_+ = u_-, \; v_+ = v_- = 0, \quad \text{for} \quad x = 1, \tag{7}$$

which enforces the flow leaves the hydrofoil tangentially and smoothly, at its cusped trailing edge.

We use the arc length s to parameterize the interface, i.e., $[x, y(x)] = [x(s), y(s)]$, then the functions $x(s)$ and $y(s)$ satisfy

$$\left(\frac{dx}{ds}\right)^2 + \left(\frac{dy}{ds}\right)^2 = 1. \tag{8}$$

The kinematic conditions on the interface become

$$\frac{d\psi_1}{ds} = \frac{d\psi_2}{ds} = 0. \tag{9}$$

The velocity components on the interface are

$$u_j = \frac{dx}{ds}\frac{d\phi_j}{ds}, \quad v_j = \frac{dy}{ds}\frac{d\phi_j}{ds}, \quad j = 1, 2,$$

The dynamic pressures p_1 and p_2 of the fluids in the upper layer and the lower layer satisfy Bernoulli's equations as follows, respectively:

$$p_1 + \frac{1}{2}\rho\left(\frac{d\phi_1}{ds}\right)^2 + \frac{\rho y}{F^2} = \frac{1}{2}\rho\gamma^2, \tag{10}$$

$$p_2 + \frac{1}{2}\left(\frac{d\phi_2}{ds}\right)^2 + \frac{y}{F^2} = \frac{1}{2}. \tag{11}$$

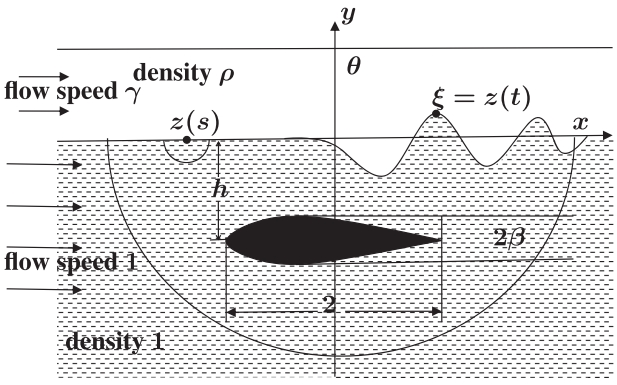

FIG. 1. Sketch of a two-layer fluid with a hydrofoil in the lower layer and the coordinate system used. The dimensionless densities of the lower and upper layers are 1 and ρ, and the speeds are 1 and γ, respectively. The dimensionless depth and thickness of the hydrofoil are h and 2β.

On the interface $y = \eta(x)$, $p_1 = p_2$, combining this with (10) and (11), gives

$$\rho\left(\frac{d\phi_1}{ds}\right)^2 - \left(\frac{d\phi_2}{ds}\right)^2 + \frac{2(\rho-1)y}{F^2} - \rho\gamma^2 + 1 = 0. \tag{12}$$

Introduce an analytic function $G(z)$ in terms of the complex potential $f_1(z)$,

$$G(z) = \frac{df_1}{dz} - \gamma.$$

Applying the Cauchy integral formula to the analytical function $G(z)$, we obtain

$$\pi \mathrm{i} G(z) = \oint_{\Gamma_1} \frac{G(\xi)}{\xi - z} d\xi, \tag{13}$$

where Γ_1 is the closed contour consisting of the interface with a semi-circular path of an infinitively small radius centered at the point $z(s)$, the image of the interface with respect to the lid $y = \theta$, and the vertical lines $x = \pm E$, as $E \to \infty$, which connect the interface and its image.

The integration along the two vertical lines is zero due to the asymptotic property of the function $G(z)$. The closed contour integration in (13) is thus reduced to the integration along the entire interface and its image. By using the boundary condition (3) on the rigid lid, (13) can be rewritten as

$$\pi \mathrm{i} G(z(s)) = \fint_{-\infty}^{\infty} \frac{G(z(\tau))z'(\tau)}{z(\tau) - z(s)} d\tau - \int_{-\infty}^{\infty} \frac{G(\tilde{z}(\tau))\tilde{z}'(\tau)}{\tilde{z}(\tau) - z(s)} d\tau, \tag{14}$$

where $z(\tau)$ is a field point at the interface and $\tilde{z}(\tau)$ is the corresponding point on the image of interface respect to $y = \theta$. Let the coordinate of the point $z(\tau)$ be $[x(\tau), y(\tau)]$, then the coordinate of the corresponding point $\tilde{z}(\tau)$ is $[x(\tau), 2\theta - y(\tau)]$.

The imaginary part of (14) gives

$$\begin{aligned} -\pi[\phi_1'(s)x'(s) - \gamma] = &\fint_{-\infty}^{\infty} \frac{[\phi_1'(\tau) - \gamma x'(\tau)][y(\tau) - y(s)] + \gamma y'(\tau)[x(\tau) - x(s)]}{[x(\tau) - x(s)]^2 + [y(\tau) - y(s)]^2} d\tau \\ &+ \fint_{-\infty}^{\infty} \frac{[\phi_1'(\tau) - \gamma x'(\tau)][y(\tau) + y(s) - 2\theta] + \gamma y'(\tau)[x(\tau) - x(s)]}{[x(\tau) - x(s)]^2 + [2\theta - y(\tau) - y(s)]^2} d\tau, \end{aligned} \tag{15}$$

where we used the kinematic condition (9) on the interface and arc length relation (8).

For the lower infinite depth layer flow, we consider the analytical function

$$F(z) = \frac{df_2}{dz} - 1.$$

According to the Cauchy integral formula, we have

$$\pi \mathrm{i} F(z) = \oint_{\Gamma_2} \frac{F(\xi)}{\xi - z} d\xi, \tag{16}$$

where the contour Γ_2 consists of the entire interface with a semi-circular path of an infinitively small radius centered at the point $z(s)$, the surface of hydrofoil, and a semi-circle centered at the origin with a radius extending to infinity. Similar to (14), we can show that the function $F(z)$ satisfies

$$\pi \mathrm{i} F(z(s)) = -\fint_{-\infty}^{\infty} \frac{F(z(\tau))z'(\tau)}{z(\tau) - z(s)} d\tau + \oint_{body} \frac{F(\lambda)}{\lambda - z} d\lambda, \tag{17}$$

where $z(s)$ is a field point along the interface, and must be by-passed with a semi-circle of a vanishingly small radius, on which the integral contribution is $-\pi \mathrm{i} F(z(s))$. The integral path around the body is to be taken clockwise. The contribution of the integration around the infinitely large semi-circle is zero according to the far field condition (2) of f_2.

The complex variable $\lambda = x + \mathrm{i} b_{\pm}(x)$ in (17) defines the hydrofoil surface, so the body integral can be written as

$$\int_{-1}^{1} \frac{(u_+ - 1 - \mathrm{i} v_+)(1 + \mathrm{i} b_+')}{\xi + \mathrm{i} b_+ - z(s)} d\xi - \int_{-1}^{1} \frac{(u_- - 1 - \mathrm{i} v_-)(1 + \mathrm{i} b_-')}{\xi + \mathrm{i} b_- - z(s)} d\xi. \tag{18}$$

To handle the inverse square-root singularities in these integrands as $x \to -1$, introduced by the functions $b_{\pm}'(x)$, we make the change of variable

$$x = k^2 - 1. \tag{19}$$

Accordingly, $b_{\pm}(x)$ can be expressed in terms of k

$$\begin{aligned} b_{\pm}(x) &= B_{\pm}(k) = -h \pm \frac{3}{4}\beta\sqrt{\frac{3}{2}}k\left(2 - k^2\right), \\ b_{\pm}'(x) &= D_{\pm}(k) = \pm\frac{3\beta}{8}\sqrt{\frac{3}{2}}\left(\frac{2 - 3k^2}{k}\right). \end{aligned} \tag{20}$$

The integral differential equation for a field point on the interface is obtained by taking the imaginary part of (17),

$$\begin{aligned} \pi[\phi_2'(s)x'(s) - 1] = &\fint_{-\infty}^{\infty} \frac{[\phi_2'(\tau) - x'(\tau)][y(\tau) - y(s)] + y'(\tau)[x(\tau) - x(s)]}{[x(\tau) - x(s)]^2 + [y(\tau) - y(s)]^2} d\tau \\ &- 2\int_0^{\sqrt{2}} \frac{[B_+(K) - y(s)][u_+ - 1 + v_+ D_+] + [K^2 - 1 - x(s)]D_+(K)}{[K^2 - 1 - x(s)]^2 + [B_+(K) - y(s)]^2} K dK \\ &+ 2\int_0^{\sqrt{2}} \frac{[B_-(K) - y(s)][u_- - 1 + v_- D_-] + [K^2 - 1 - x(s)]D_-(K)}{[K^2 - 1 - x(s)]^2 + [B_-(K) - y(s)]^2} K dK, \end{aligned} \tag{21}$$

where we used the boundary conditions (5) on the hydrofoil surface, the kinematic condition (9) on the interface, and the natural arc length relation (8). To get the unknown quantities $u_\pm$ in (21), the integration path is replaced by a semi-circle with a vanishingly small radius excluding the field point $z = z^* = x^* + \mathrm{i}y^* = k^2 - 1 + \mathrm{i}B_\pm(k)$ on the hydrofoil, thus (21) becomes

$$\begin{aligned}\pi C[u_\pm(k) - 1] = &\int_{-\infty}^{\infty} \frac{[\phi_2'(\tau) - x'(\tau)][y(\tau) - B_\pm(k)] + y'(\tau)[x(\tau) - k^2 + 1]}{[x(\tau) - k^2 + 1]^2 + [y(\tau) - B_\pm(k)]^2} d\tau \\ &- 2 \oint_0^{\sqrt{2}} \frac{[B_+(K) - B_\pm(k)][u_+ - 1 + v_+ D_+] + [K^2 - k^2] D_+(K)}{[K^2 - k^2]^2 + [B_+(K) - B_\pm(k)]^2} K dK \\ &+ 2 \oint_0^{\sqrt{2}} \frac{[B_-(K) - B_\pm(k)][u_- - 1 + v_- D_-] + [K^2 - k^2] D_-(K)}{[K^2 - k^2]^2 + [B_-(K) - B_\pm(k)]^2} K dK, \end{aligned} \tag{22}$$

where C is equal to unit, except for the trailing edge for $k = \sqrt{2}$. For the latter case, C is equal to the value $2 - \frac{\delta}{\pi}$, where δ is the cusped angle at the trailing edge.

Governing equations for the problem consist of (8), (12), (15), (21), and (22), subject to the far field conditions (2) and the Kutta condition (7).

For $\rho = 0$ in the upper layer flow, two-layer flows become one single layer flow. The five governing equations will degenerate into four governing equations proposed in Ref. 31. The numerical results for $\rho = 0$, which will be shown in Subsec. IV B, also agree well with the results obtained in Ref. 31.

III. NUMERICAL MODELLING

The numerical method is implemented based on the quasi-Newton method. The computational domain $(-\infty, +\infty)$ of the interface is truncated to $[E_1, E_2]$, then it is discretized as N evenly distributed grids,

$$s_i = E_1 + (i-1)\Delta s, i = 1, \ldots, N, \tag{23}$$

where $\Delta s = \frac{E_2 - E_1}{N-1}$. The hydrofoil surface is represented by M evenly distributed grids

$$k_i = k_1 + (i-1)\Delta h, i = 1, \ldots, M, \tag{24}$$

where $\Delta h = \frac{k_M - k_1}{M-1}$.

The unknown quantities $x(s), y(s), \phi_1(s)$ and $\phi_2(s)$ for $s = s_i$ on the interface are denoted as $x_i, y_i, \phi_1(s_i)$ and $\phi_2(s_i)$. The discretized velocity components on the hydrofoil surface are denoted as u_i^+, u_i^-, v_i^+, and v_i^-. To remove the singularity of integration, $N-1$ midpoints are calculated,

$$s_{i-\frac{1}{2}} = \frac{1}{2}(s_{i-1} + s_i), i = 2, \ldots, N. \tag{25}$$

The value of $x(s)$ at the midpoint $s_{i-\frac{1}{2}}$ can be approximated as

$$x_{i-\frac{1}{2}} = \frac{1}{2}(x_{i-1} + x_i), i = 2, \ldots, N.$$

Similarly, the values of $y(s), x'(s), y'(s), \phi_1'(s), \phi_2'(s)$ at $s_{i-\frac{1}{2}}$ can be given.

To satisfy the far field conditions (2) and Bernoulli's equation (10) and (11), we take

$$\begin{aligned} &y_1 = y_1' = 0, \quad x_1' = 1, \quad x_1 = \phi_j(s_1) = s_1, \\ &j = 1, 2, \quad \phi_1'(s_1) = \gamma, \quad \phi_2'(s_1) = 1. \end{aligned} \tag{26}$$

The initial guess of the solutions of $y_2', y_3', \ldots, y_N'$ are needed and set as zero. The quantities x_i' can be calculated using arc length relation, and the quantities $x_i, y_i, \phi_j(s_i), j = 1, 2$ can be calculated using trapezoidal rule integration. The non-penetration boundary condition (5) at the hydrofoil surface and the Kutta condition (7) at its trailing edge are also imposed following Ref. 31.

After the above procedures, the integral functions in (15) are evaluated at the midpoints $s_{i-\frac{1}{2}}, i = 2, \ldots, N$, and the integral are computed approximately by the trapezoidal rule. This yields a system of linear algebraic equations for $\phi_1'(s_i), i = 2, \ldots, N$.

$$\begin{aligned} -[\phi_1'(s_{i-\frac{1}{2}}) x'_{i-\frac{1}{2}} - \gamma] = &\frac{\Delta s}{\pi} \sum_{j=1}^{N} w_j \frac{[\phi_1'(s_j) - \gamma x_j'](y_j - y_{i-\frac{1}{2}}) + \gamma y_j'(x_j - x_{i-\frac{1}{2}})}{[x_j - x_{i-\frac{1}{2}}]^2 + [y_j - y_{i-\frac{1}{2}}]^2} \\ &+ \frac{\Delta s}{\pi} \sum_{j=1}^{N} w_j \frac{[\phi_1'(s_j) - \gamma x_j'](y_j - y_{i-\frac{1}{2}} - 2\theta) + \gamma y_j'(x_j - x_{i-\frac{1}{2}})}{[x_j - x_{i-\frac{1}{2}}]^2 + [2\theta - y_j - y_{i-\frac{1}{2}}]^2}, \\ &i = 2, 3, \ldots, N, \end{aligned} \tag{27}$$

where $w_1 = w_N = \frac{1}{2}$ and $w_j = 1, j = 2, 3, \ldots, N-1$. $\phi_2'(s_i)$ can be obtained from (12),

$$\phi_2'(s_i) = \left(\rho[\phi_1'(s_i)]^2 + \frac{2(\rho - 1) y_i}{F^2} - \rho\gamma^2 + 1 \right)^{\frac{1}{2}}. \tag{28}$$

Now that the integral equation (22) is discretized as $2M-2$ algebraic equations. In view of the Kutta condition (7), we define the vector $\mathbf{U} = [v_1^\pm, u_2^+, \ldots, u_{M-1}^+, u_M^\pm, u_2^-, \ldots, u_{M-1}^-]$. To eliminate the normal component of velocity, $v_i^\pm$ can be written in the form of

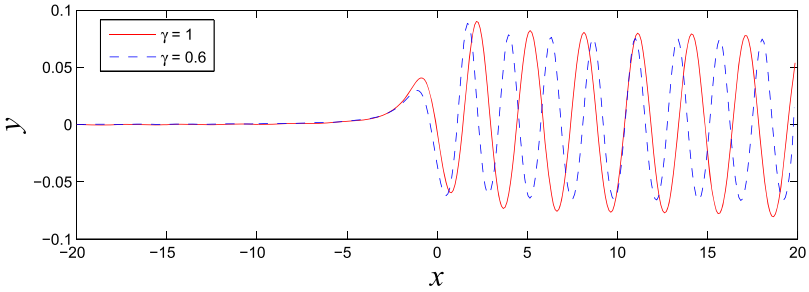

FIG. 2. The wave profile of the internal wave at the interface of a two-layer flow, for $h = 1$, $\beta = 0.15$, $F = 0.4$, $\rho = 0.5$ and $\gamma = 0.6$ (dashed line), and $\gamma = 1$ (solid line).

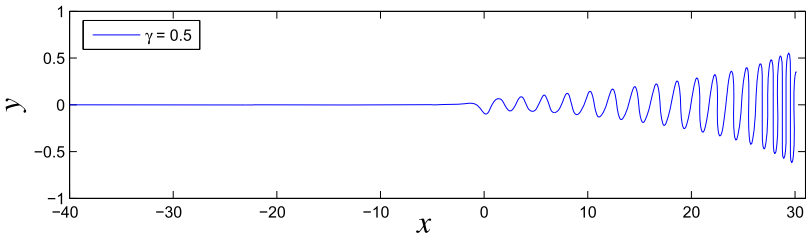

FIG. 3. The wave profile of the internal wave at the interface of a two-layer flow, for $h = 1$, $\beta = 0.15$, $F = 0.4$, $\rho = 0.5$, and $\gamma = 0.5$.

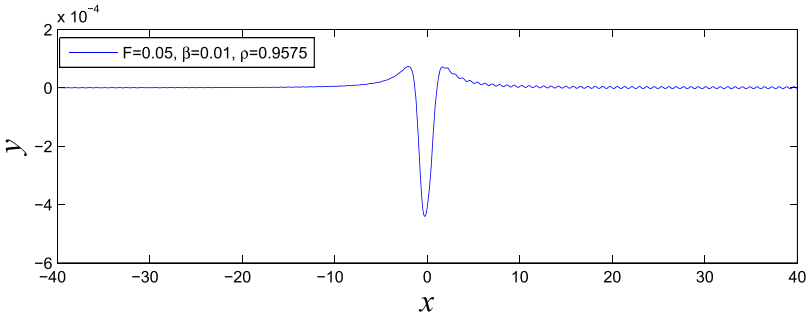

FIG. 4. The wave profile of the internal wave at the interface of a two-layer flow, for $h = 1$, $\beta = 0.01$, $F = 0.05$, and $\rho = 0.9575$.

$$v_i^+ = u_i^+ D_+(k_i), \quad v_i^- = u_i^- D_-(k_i), \quad i = 2, \ldots, M-1, \quad (29)$$

by using the boundary condition on the hydrofoil surface (5). The integral equation (22) yields the discrete algebraic equations, which can be expressed in a matrix form,

$$\mathbf{SU} = \mathbf{TU} + \mathbf{R}, \quad (30)$$

where $\mathbf{S}$ and $\mathbf{T}$ are $(2M-2) \times (2M-2)$ matrices and $\mathbf{R}$ is a vector whose length is $2M-2$. We also should note that $(\mathbf{S}-\mathbf{T})^{-1}$ does not change during the iteration.

Since all values of unknown quantities are provided, the residual errors Q_i can be computed by the discrete form of integro-differential equation (21) at the interface, which can be re-written as a set of nonlinear equations in terms of $\mathbf{y}' = [y_2', y_3', \ldots, y_N']^T$,

$$Q_i(\mathbf{y}') = 0, \quad i = 2, 3, \ldots, N. \quad (31)$$

We can solve (31) using the quasi-Newton iteration method to update $\mathbf{y}' = [y_2', y_3', \ldots, y_N']^T$, unless the Euclidean norm $\|\mathbf{Q}\|$ of the vector of residual errors is sufficiently small. Denoting the k-th iteration solution as $y_j'^{(k)}$, $j = 2, 3, \ldots, N$, we have $y_j'^{(k+1)} = y_j'^{(k)} + \Delta_j^{(k)}$, $j = 2, 3, \ldots, N$, where the correction vector $[\Delta_2^{(k)}, \Delta_3^{(k)}, \ldots, \Delta_N^{(k)}]^T$ satisfies

$$\sum_{j=2}^{N} \left(\frac{\partial Q_i}{\partial y_j'} \right)^{(k)} \Delta_j^{(k)} = -Q_i^{(k)}, \quad i = 2, 3, \ldots, N. \quad (32)$$

The Jacobian matrix of derivatives in (32) can be computed by the forward difference method. In this paper, we use the quasi-Newton method coupled with Broyden's rank one method[35] to update the correction vector and $[y_2', y_3', \ldots, y_N']^T$.

IV. NUMERICAL RESULTS

A. Wave profiles

The parameters used for calculations are as follows: the dimensionless depth of the upper layer $\theta = 20$, grids used for the hydrofoil $M = 101$, and convergence precision $\varepsilon = 10^{-8}$. The computations were done on a computer with a central processing unit (CPU): Intel(R) Core(TM) i7-4790 and converge to a highly accurate solution of the integro-differential equations within thirteen iterations of the quasi-Newton method.

Figure 2 shows the typical interface wave profiles computed with the numerical method. 400 grids are used for the interval [−20, 20] to calculate the wave profiles with the depth of hydrofoil $h = 1$, half-thickness of hydrofoil $\beta = 0.15$, Froude number $F = 0.4$, and density ratio $\rho = 0.5$, the dimensionless velocity $\gamma = 0.6$, and $\gamma = 1$. The interface rises on the nose of the hydrofoil and falls above the tail. The following second crest (trough) is much more prominent than the first crest (trough). The wave is stabilized quickly subsequently.

TABLE I. Comparison of Newton's method and the quasi-Newton method for the same convergence precision $\varepsilon = 10^{-8}$, and $h = 1$, $\beta = 0.15$, $F = 0.4$, and $\rho = 0.5$.

Methods	Domain	M	N	Iterations	CPU Time(s)
Newton's method	[−20,20]	101	201	7	1387.20
Quasi-Newton method	[−20,20]	101	201	13	221.13

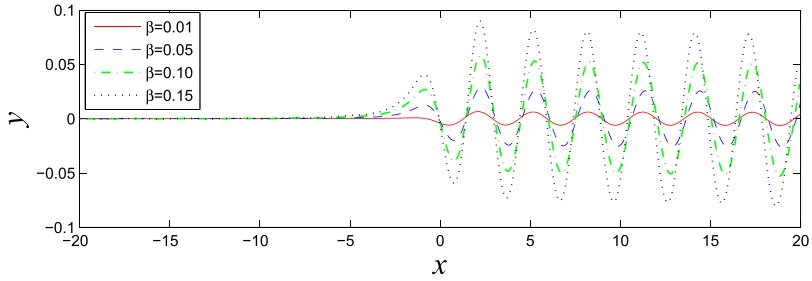

FIG. 5. The internal wave profiles for various half-thickness of the hydrofoil $\beta = 0.01, 0.05, 0.10, 0.15$, and $h = 1$, $F = 0.4$ and $\rho = 0.5$.

In Fig. 2, we compare the interface wave profiles for $\gamma = 0.6$ and 1.0. The wavelength for $\gamma = 1$ is larger than that for $\gamma = 0.6$. Instability can occur when the density of the upper layer is greater than that of lower layer or there is a large velocity difference across the interface between two fluids or there is a short wave. Figure 3 shows the unstable interface

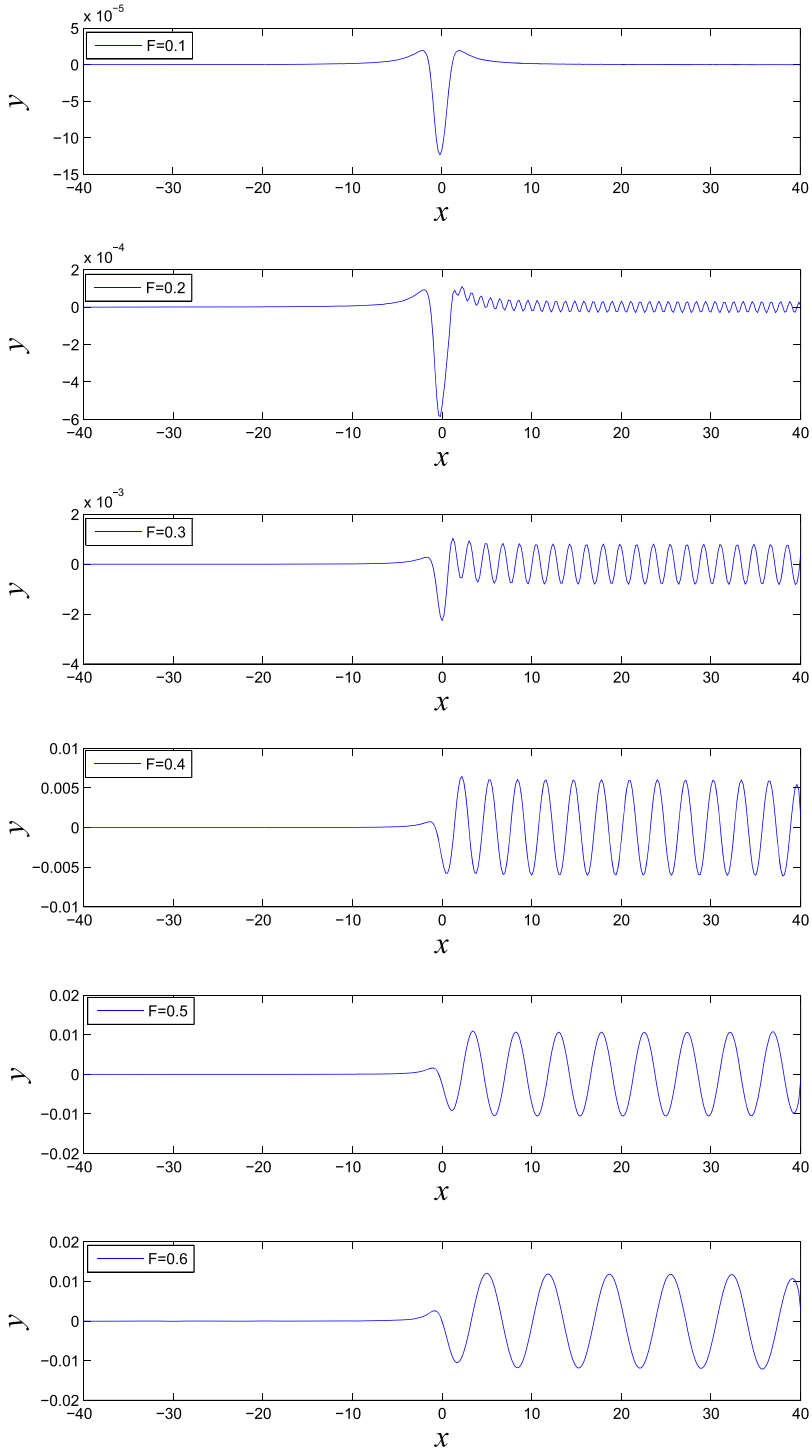

FIG. 6. Internal wave profiles for different Froude numbers $F = 0.1, 0.2, 0.3, 0.4, 0.5, 0.6$, and $h = 1$, $\beta = 0.01$ and $\rho = 0.5$.

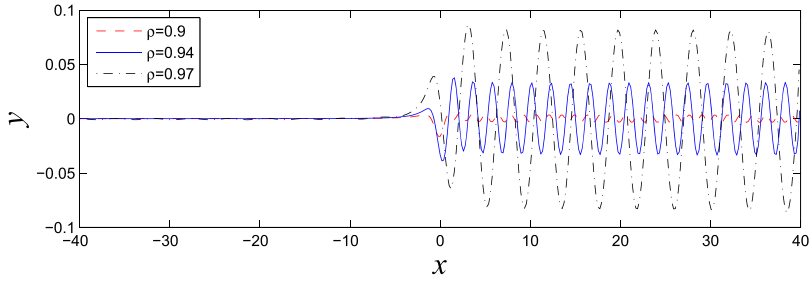

FIG. 7. Internal wave profiles for three different density ratios $\rho = 0.90, 0.94, 0.97$, and $F = 0.1$, $h = 1$ and $\beta = 0.15$.

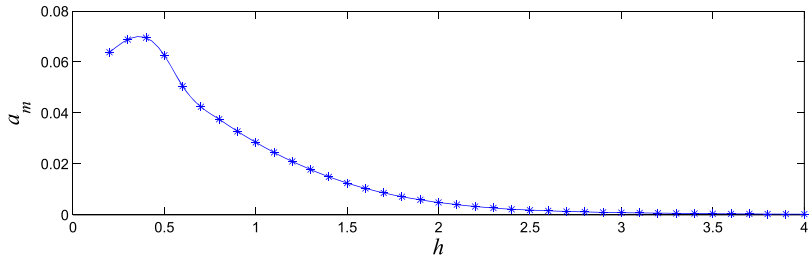

FIG. 8. The maximum internal wave amplitude a_m versus the dimensionless depth h of the hydrofoil, for $F = 0.4, \beta = 0.05$ and $\rho = 0.5$.

wave profile with $\gamma = 0.5$ and the remaining parameters are the same as in Fig. 2. When $\gamma = 0.5$, the Kelvin-Helmholtz instability might occur in unsteady flow. The same speed of the upper layer and lower layer, i.e., the dimensionless velocity $\gamma = 1$ is set, without loss of generality.

Figure 4 shows an interesting wave whose type is similar to a solitary wave at the interface, for $h = 1$, $\beta = 0.01$, $F = 0.05$, and $\rho = 0.9575$. 1600 grids are used for the computational interval $[-40, 40]$ to calculate the wave profile. Through careful observation, it can be observed that there is a train of an extremely small wave downstream under the high precision numerical scheme.

Table I shows the comparison between Newton's method and the quasi-Newton method for a typical example with the parameters $h = 1$, $\beta = 0.15$, $F = 0.4$, and $\rho = 0.5$. We set same computational domain and grids at the interface and hydrofoil surface for both methods. Table I shows the iterations and CPU time of Newton's method and the quasi-Newton method for same accuracy. The quasi-Newton method needs more iterations to reach the same accuracy of Newton's method. But it only costs about one-seventh of the CPU time of Newton's method. In the quasi-Newton method, the Jacobian matrix is calculated once per time step, while in Newton's method, the Jacobian matrix is calculated for every iteration.

Figure 5 displays the wave profile at various half-thickness β of the hydrofoil, with the remaining parameters kept the same as in Fig. 2. The wave amplitude increases with the hydrofoil thickness while the wavelength does not change significantly.

Figure 6 displays the effects of the Froude number on the wave profiles, for $h = 1$, $\beta = 0.01$ and $\rho = 0.5$. The amplitudes and wavelengths of the downstream waves increase with the Froude number. As $F < 0.4$, the first troughs of wave profiles are bigger than others, whereas as $F \geqslant 0.4$, the first troughs have similar amplitudes to others.

Figure 7 shows the wave profiles for $\rho = 0.90, 0.94, 0.97$, and $F = 0.1, h = 1$, and $\beta = 0.15$. The largest wave corresponds to $\rho = 0.97$, which is a typical value used for analyzing internal waves in the ocean. The wave amplitude and wavelength increase significantly with the density ratio. The wave amplitude and wavelength for $\rho = 0.97$ are more than twice that for $\rho = 0.94$.

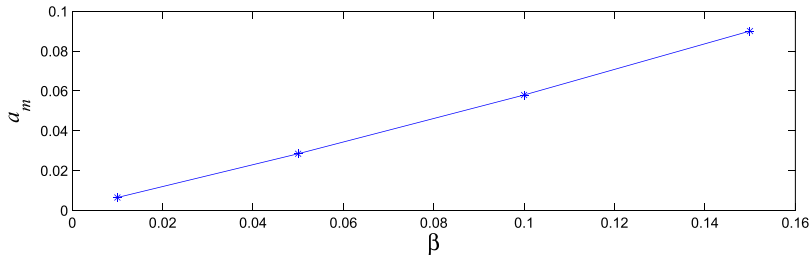

FIG. 9. The maximum internal wave amplitude a_m versus the dimensionless half-thickness β of the hydrofoil, for $h = 1$, $F = 0.4$ and $\rho = 0.5$.

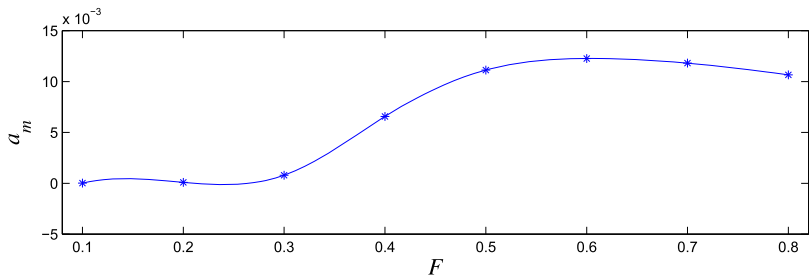

FIG. 10. The maximum internal wave amplitude a_m versus the Froude number F of the hydrofoil, for $h = 1$, $\beta = 0.01$ and $\rho = 0.5$.

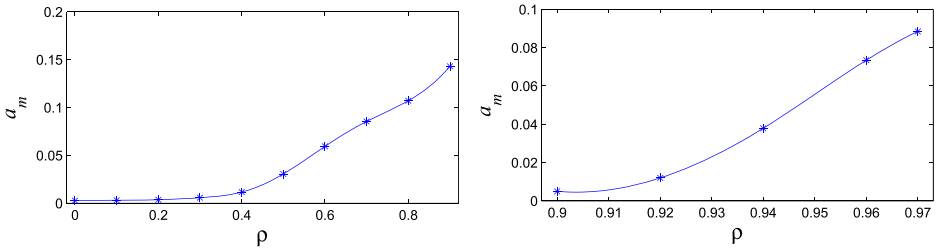

FIG. 11. The maximum internal wave amplitude a_m versus the various dimensionless density ratio ρ, the subfigure (a) is for $h = 1, \beta = 0.15$ and $F = 0.3$ when $0 \leqslant \rho \leqslant 0.9$, and the subfigure (b) is for $h = 1, \beta = 0.15$ and $F = 0.1$ when $0.9 \leqslant \rho \leqslant 0.97$.

B. Maximum amplitude

Figure 8 displays the maximum amplitude a_m of the internal wave versus the depth h of the hydrofoil, for $F = 0.4$, $\beta = 0.05$ and $\rho = 0.5$. As the depth h increases, the maximum wave amplitude firstly increases, reaching the maximum at about $h = 0.4$, and then decreases. As $h < 1$, the amplitude a_m is at the order of the thickness of the hydrofoil; however, as $h > 2$, a_m is small. It is helpful to optimize the depth of cruising in order to promote the efficiency and reduce the underwater noise in marine engineering.

Figure 9 shows the maximum amplitude a_m of internal waves versus the dimensionless half-thickness β of the hydrofoil, for $h = 1$, $F = 0.4$, and $\rho = 0.5$. The maximum wave amplitude a_m is at the same order of β and increases approximately linearly with the hydrofoil half-thickness β. This is reasonable since the disturbance of the hydrofoil increases with its thickness and the thickness considered is small.

Figure 10 shows that the maximum internal wave amplitude a_m versus the Froude number F. As the Froude number F increases, the maximum wave amplitude increases slowly with F as $F < 0.3$, increases substantially after that, reaching maximum value at about $F = 0.6$, and decreases after that.

Figure 11 shows that the maximum amplitude a_m of internal waves versus the density ratio of the upper layer to lower layer. The subfigure (a) is for $h = 1, \beta = 0.15$, and $F = 0.3$ when $0 \leqslant \rho \leqslant 0.9$, and the subfigure (b) is for $h = 1, \beta = 0.15$, and $F = 0.1$ when $0.9 \leqslant \rho \leqslant 0.97$. The wave amplitude increases monotonically with the density ratio and increases faster at a larger density ratio. For $\rho = 0$, the internal wave degenerates to a free surface wave of a single-layer fluid, and its behaviors coincide well with the results of Ref. 31 for a free surface wave. It is noticed that the amplitude of interfacial wave is much greater than that for free surface waves generated by a hydrofoil at corresponding conditions.

V. SUMMARY AND CONCLUSIONS

We are concerned with the interfacial waves generated by a submerged hydrofoil beneath the interface of a two-layer fluid. Integral-differential equations for the phenomenon are formulated for the two-layer flows using the potential flow theory coupled with complex analysis. The numerical method based on the quasi-Newton method is shown to be significantly more efficient than Newton's method. The parametric study is carried out in terms of the location and thickness of the hydrofoil, the Froude number, and the density ratio of the two layer fluids. The following features were observed for the phenomenon.

The wave profile depends on the Froude number. For the cases considered, the first troughs of wave profiles are bigger than others for $F < 0.4$ but have similar amplitudes to others for $F > 0.4$. The Kelvin-Helmholtz instability can occur when there is a large velocity difference across the interface between two fluids, in an unsteady flow.

As the thickness of the hydrofoil increases, the wave amplitude increases, and the wavelength does not change. The wave amplitude and wavelength increase significantly with the density ratio of the upper layer to lower layer. As the dimensionless depth h increases, the wave amplitude firstly increases, reaching the maximum at about $h = 0.4$, and then decreases. In particular, the amplitude of the internal wave is much greater than that of the corresponding free surface wave.

ACKNOWLEDGMENTS

This work is supported by Natural Sciences Foundation of China (Nos. 51579040, 51379033, and 51522902) and Fundamental Research Fund for the Central Universities (No. DUT16QY41). Many thanks to anonymous reviewers' helpful and constructive suggestions and comments.

[1] J. Lighthill, *Waves in Fluids* (Cambridge University Press, 2001).
[2] C. S. Yih, *Stratified Flows* (Academic Press, 1980).
[3] M. H. Alford, T. Peacock, J. A. Mackinnon *et al.*, "The formation and fate of internal waves in the South China Sea," Nature **521**, 65–69 (2015).
[4] L. V. Yuri and N. Yokoyama, "Nonlinear wave–wave interactions in stratified flows: Direct numerical simulations," Phys. D **238**(8), 803–815 (2007).
[5] J. Mackinnon, "Mountain waves in the deep ocean," Nature **501**, 321–322 (2013).
[6] S. Q. Cai, J. Xie, and J. He, "An overview of internal solitary waves in the South China Sea," Surv. Geophys. **33**, 927–943 (2012).
[7] J. T. Nault and B. R. Sutherland, "Internal wave transmission in nonuniform flows," Phys. Fluids **19**, 016601 (2007).
[8] P. G. Baines, *Topographic Effect in Stratified Flows* (Cambridge University Press, 1995).
[9] K. B. Winters and L. Armi, "Topographic control of stratified flows: Upstream jets, blocking and isolating layers," J. Fluid Mech. **753**, 80–103 (2014).
[10] J. M. Vanden-Broeck, *Gravity-Capillary Free Surface Flows* (Cambridge University Press, 2010).
[11] K. R. Helfrich and W. K. Melville, "Long nonlinear internal waves," Annu. Rev. Fluid Mech. **38**, 395–425 (2006).
[12] M. R. Alam, Y. M. Liu, and D. K. P. Yue, "Waves due to an oscillating and translating disturbance in a two layer density stratified fluid," J. Eng. Math. **65**(2), 179–200 (2009).
[13] A. Carabineanu, "The study of the potential flow past a submerged hydrofoil by the complex boundary element method," Eng. Anal. Boundary Elem. **39**(2), 23–35 (2014).
[14] G. Contento, G. Lupieri, and H. Jasak, "Numerical study of unsteady breaking waves induced by a submerged hydrofoil at steady forward speed," in *NAV 2015–18th International Conference on Ships and Shipping Research* (Organising Committee NAV, 2015); available at https://core.ac.uk/display/53745911.

[15]B. Prasad, T. Hino, and K. Suzuki, "Numerical simulation of free surface flows around shallowly submerged hydrofoil by OpenFOAM," Ocean Eng. **102**, 87–94 (2015).
[16]L. Lacaze, A. Paci, and E. Cid, "Wave patterns generated by an axisymmetric obstacle in a two-layer flow," Exp. Fluids **54**(12), 1–10 (2013).
[17]L. K. Forbes and L. W. Schwartz, "Free-surface flow over a semicircular obstruction," J. Fluid Mech. **114**, 299–314 (1982).
[18]L. K. Forbes, "On the wave resistance of a submerged semi-elliptical body," J. Eng. Math. **15**, 287–298 (1981).
[19]L. K. Forbes, "Non-linear, drag-free flow over a submerged semi-elliptical body," J. Eng. Math. **16**, 171–180 (1982).
[20]L. K. Forbes, "Two-layer critical flow over a semi-circular obstruction," J. Eng. Math. **23**, 325–342 (1989).
[21]S. R. Belward and L. K. Forbes, "Fully non-linear two-layer flow over arbitrary topography," J. Eng. Math. **27**(4), 419–432 (1993).
[22]W. K. Melville and K. R. Helfrich, "Transcritical two-layer flow over topography," J. Fluid Mech. **178**, 31–52 (1987).
[23]F. Dias and J. M. Vanden-Broeck, "Trapped waves between submerged obstacles," J. Fluid Mech. **509**, 93–102 (2004).
[24]C. Page and E. I. Parau, "Hydraulic falls under a floating ice plate due to submerged obstructions," J. Fluid Mech. **745**, 208–222 (2014).
[25]E. I. Parau, J. M. Vanden-Broeck, and M. J. Cooker, "Time evolution of three-dimensional nonlinear gravity–capillary free-surface flows," J. Eng. Math. **68**, 291–300 (2010).
[26]Q. X. Wang, "Unstructured MEL modelling of unsteady nonlinear ship waves," J. Comput. Phys. **210**(1), 368–385 (2005).
[27]G. C. Hocking and L. K. Forbes, "Super-critical withdrawal from a two-layer fluid through a line sink if the lower layer is of finite depth," J. Fluid Mech. **428**, 333–348 (2001).
[28]L. K. Forbes and J. M. Cosgrove, "A line vortex in a two-fluid system," J. Eng. Math. **84**, 181–199 (2014).
[29]T. E. Stokes, G. C. Hocking, and L. K. Forbes, "Steady free surface flows induced by a submerged ring source or sink," J. Fluid Mech. **694**, 352–370 (2012).
[30]Z. Wang, L. Zou, H. Liang, and Z. Zong, "Nonlinear steady two layer interfacial flow about a submerged point vortex," J. Eng. Math. **103**, 39–53 (2017).
[31]L. K. Forbes, "A numerical method for non-linear flow about a submerged hydrofoil," J. Eng. Math. **19**, 329–339 (1985).
[32]L. K. Forbes and G. C. Hocking, "Flow due to a sink near a vertical wall, in infinitely deep fluid," Comput. Fluids **34**(6), 684–704 (2005).
[33]R. Pethiyagoda, S. W. McCue, and T. J. Moroney, "What is the angle of a nonlinear Kelvin ship wave pattern?," J. Fluid Mech. **758**, 468–485 (2014).
[34]F. M. Hassen, "Boundary integral method applied to the propagation of non-linear gravity waves generated by a moving bottom," Appl. Math. Modell. **33**, 451–466 (2009).
[35]C. G. Broyden, "A class of methods for solving nonlinear simultaneous equations," Math. Comput. **19**(2), 577–593 (1965).